J. Fluid Mech. (2023), *vol*. 969, A34, doi:10.1017/jfm.2023.593

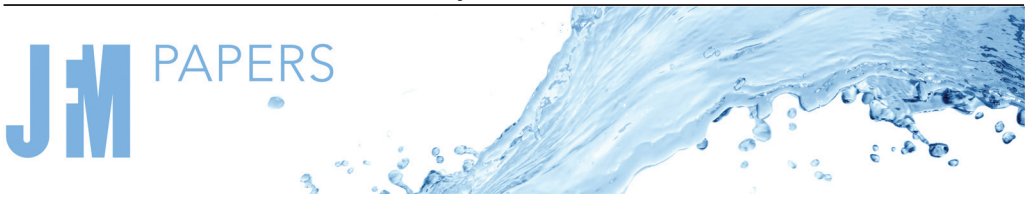

Swimming of an inertial squirmer and squirmer dumbbell through a viscoelastic fluid

Zhenyu Ouyang[1], Zhaowu Lin[2,†], Jianzhong Lin[1,2,†], Nhan Phan-Thien[3] and Jue Zhu[1]

[1]Laboratory of Impact and Safety Engineering (Ningbo University), Ministry of Education, 315201 Ningbo, China

[2]Department of Mechanics, State Key Laboratory of Fluid Power and Mechatronic Systems, Zhejiang University, 310027 Hangzhou, China

[3]Department of Mechanical Engineering, National University of Singapore, Singapore 117575, Singapore

(Received 19 February 2023; revised 18 May 2023; accepted 16 July 2023)

We investigate the hydrodynamics of a spherical and dumbbell-shaped swimmer in a viscoelastic fluid, modelled by the Giesekus constitutive equation. The 'squirmer', a model of a micro-swimmer with tangential surface waves at its boundaries, is simulated utilizing a direct-forcing fictitious domain method. We consider the competitive effects of the fluid inertia and elasticity on the locomotion of the swimmers. For the neutral squirmer, its speed increases monotonically with increasing Reynolds number in the Giesekus fluid, in contrast to holding a constant speed in a Newtonian one. Meanwhile, the speed of the finite inertial squirmer increases monotonically with fluid elasticity, as measured by the Weissenberg number. Regarding the dumbbell-shaped swimmers in the Giesekus fluid, we find the pusher–puller (the puller is in front of the pusher) dumbbell swimming to be significantly faster than other dumbbells, providing practical guidance in assembling the complex micro-swimming devices. We further consider the squirmer's (or the dumbbell-shaped squirmer's) energy expenditure and hydrodynamic efficiency, finding that swimming in viscoelastic fluids expends less energy than its Newtonian counterpart, and the neutral squirmer expends more energy than a pusher or puller. The energy expenditure and hydrodynamic efficiency are relevant to steady swimming speeds, in which a faster counterpart squirmer (dumbbell-shaped squirmer) expends less energy but has higher hydrodynamic efficiency.

Key words: suspensions, viscoelasticity, particle/fluid flows

† Email addresses for correspondence: linzhaowu@zju.edu.cn, mecjzlin@public.zju.edu.cn

1. Introduction

Recently, the motion of micro-swimmers in complex fluids has attracted a considerable attention as it is relevant in medicine, ecology and technological applications (Datt *et al.* 2017; Li, Lauga & Ardekani 2021). Examples of this problem include the locomotion of mammalian spermatozoa in viscoelastic mucus (Katz & Berger 1980), the Lyme disease spirochete *Borrelia burgdorferi* penetrating the extracellular matrix of mammalian skin (Harman *et al.* 2012), bacteria producing extracellular polymeric substances and forming biofilms (Costerton *et al.* 1987). A proper understanding of the micro-swimmer's hydrodynamics in these environments is not only interesting from a scientific perspective, but also plays a significant role in designing efficient swimming devices relevant for drug delivery (Gao & Wang 2014), gene therapy and bionic (Yan *et al.* 2017) applications (Li *et al.* 2017*a*).

The complex carrier fluid can significantly affect the swimming behaviour of the individual micro-swimmers. For example, the bacteria *Chlamydomonas reinhardtii* and *E. coli* can swim significantly faster in viscoelastic fluids or a polymer solution than in a Newtonian fluid, and *E. coli* follows straighter trajectories in the polymer solution because of the suppressed wobbling of the cell body (Patteson *et al.* 2015; Li *et al.* 2017*b*). In contrast, the algal cell *C. reinhardtii* is hindered in a viscoelastic fluid than in a Newtonian fluid as the viscoelasticity restricts the displacement of the flagella near the cell body (Smith *et al.* 2009). It is concluded that fluid viscoelasticity affects the swimming ability (both hastens and hinders) of an organism depending on its self-propelling mode (Elfring & Goyal 2016), the structural properties of the body (Zhu *et al.* 2011) and the rheological behaviour of the surrounding fluid (Dasgupta *et al.* 2013). A classical 'squirmer' is widely employed to investigate the swimming of a micro-swimmer through a viscoelastic and shear-dependent medium. This model was proposed by Lighthill (1952) and extended by Blake (1971), and it has been successfully used to mimic the self-propulsion of a swimmer with a dense array of cilia on its surface, such as *Opalina* and *Volvox* (Pedley, Brumley & Goldstein 2016). The studied scenarios include the self-propelled organisms' nutrient uptake (Magar, Goto & Pedley 2003; Magar & Pedley 2005), their hydrodynamic interactions with a wall (Ishimoto & Gaffney 2013; Ouyang, Lin & Ku 2018*a*), the two-body hydrodynamic interactions (Ishikawa, Simmonds & Pedley 2006; Götze & Gompper 2010; Navarro & Pagonabarraga 2010; Ouyang, Lin & Ku 2019) and their collective swimming dynamics (Ishikawa, Locsei & Pedley 2008; Ishikawa & Pedley, 2008; Zöttl & Stark 2014). Zhu *et al.* (2011) numerically study the steady locomotion of a neutral squirmer in a Giesekus fluid (a viscoelastic fluid model) at a low Reynolds number, finding that the viscoelasticity leads to a slower speed than in a Newtonian fluid, and a minimum speed occurs at a Weissenberg number of order 1. They also find a higher swimming efficiency in the polymeric fluid than in the Newtonian fluid. This also applies to the pusher and puller, reported in their subsequent study (Zhu, Lauga & Brandt 2012). Recently, Binagia *et al.* (2020) propose an alternative mechanism for enhancing the speed of a squirmer by coupling the fluid elasticity and local swirling flow induced by the azimuthal term of the squirmer model. This azimuthal term generates no net change of the squirmer's speed in a Newtonian fluid in the Stokes regime ($Re = 0$), but can significantly affect the speed by altering the flow structure behind the squirmer in a viscoelastic fluid (Binagia *et al.* 2020; Housiadas 2021; Housiadas, Binagia & Shaqfeh 2021). In a shear-thinning fluid, the swirling flow can either increase or decrease the squirmer's speed depending on the Carreau number (Nganguia *et al.* 2020).

Even though several case studies for a micro-swimmer through a non-Newtonian fluid have been made, these are in the limit of the Stokes flow regime (neglecting the effect

of fluid inertia). Actually, some aquatic micro-swimmers can swim at a finite Reynolds number in the range of O (1–100) (Childress 1981; Beckett 1986; Kiørboe, Jiang & Colin 2010; Wickramarathna, Noss & Lorke 2014), where the fluid inertia can play a significant role in their escape from a predator. Recent efforts indicate that the finite fluid inertia has a remarkable effect on the squirmer's locomotion, both enhancing or hindering the speed of the swimmer (Wang & Ardekani 2012; Khair & Chisholm, 2014; Ouyang, Lin & Ku 2018*b*; More & Ardekani, 2020), destabilizing the pusher (Chisholm *et al.* 2016; Li, Ostace & Ardekani 2016), changing the contact time with a wall (Ouyang *et al.* 2018*a*) and weakening the collective dynamics (Lin & Gao 2019). One may then ask how the fluid inertia and elasticity can competitively or synergistically affect the swimming speed or hydrodynamic efficiency of a squirmer, which is a model of microorganisms.

Many microorganisms in nature are non-spherical in shape (Schaller *et al.* 2010; Sanchez *et al.* 2012; Wensink *et al.* 2012), and the design of micro-swimming devices should not be focused solely on the simple spherical shape. One alternative and efficient solution in forming more complex autonomous micro-robots (Ishikawa 2019) and new functional soft materials (Cates & MacKintosh 2011; Winkler & Gompper 2020) is to construct several spherical swimmers appropriately and link them together. A typical assembly that draws attention is the squirmer dumbbell or rod, assembled by two or more squirmers in tandem. A recent investigation concerning a squirmer dumbbell's stability (Ishikawa 2019) and its swimming behaviour has been conducted (Clopés, Gompper & Winkler 2020, 2022). Their results indicate that a pusher (propelled by the rear) is more stable and efficient than a puller (propelled by the front); they also reveal a strong influence of the squirmers' flow fields on the orientation of their propulsion directions and the swimming behaviour of a dumbbell. Zantop & Stark (2020) conclude that a squirmer rod can generate a flow structure with four hydrodynamic moments, including a force dipole, source dipole, force quadrupole and source octupole. Their efforts still focus on swimming in the Newtonian and Stokes flow regimes. At a finite Re, the swimming speed and hydrodynamic efficiency of a dumbbell or rod are different from those of an individual squirmer as the flow structure is modified by the hydrodynamic interaction between the squirmers of the assembly (Ouyang & Lin 2021; Ouyang & Phan-Thien 2021; Ouyang *et al.* 2022). However, it is largely unexplored how the fluid viscoelasticity modifies the hydrodynamic interaction between the squirmers, consequently affecting the assembly's swimming speed and hydrodynamic efficiency.

This paper employs a direct-forcing fictitious domain method (DF-FDM) to investigate a spherical and a dumbbell-shaped swimmer in an infinite viscoelastic fluid. The main aim of this study is to elucidate how the fluid inertia, elasticity and the arrangement of the squirmers competitively affect the swimmer's hydrodynamics. Another aim is to arrive at potentially the most efficient swimmer in a complex viscoelastic fluid. The remainder of this paper is organized as follows. Section 2 briefly states the DF-FDM and the dynamics of the squirmer and the squirmer dumbbell. Subsequently, we validate the steady speed of an individual squirmer through Giesekus fluids ($Re = 0$) against the available results. Section 4 presents the results, including the swimmers' swimming speeds, the force contribution analysis and their energy expenditure and hydrodynamic efficiency. In section 5, some concluding remarks are finally given.

2. Numerical method and swimming model

The interface-resolved DF-FDM proposed by Yu & Shao (2007) is adopted here to simulate a spherical and a dumbbell squirmer swimming in a viscoelastic fluid.

This method fills the interior of the body with a fictitious fluid, and a pseudo-body force is considered over the body inner domain to force the fictitious fluid to satisfy the rigid-body motion constraint when coping with hydrodynamic interactions between the body and the fluid. For simplicity, we demonstrate the following non-dimensional fictitious domain formulation for an incompressible fluid which contains three parts. Let P_0 denote the solid domain and Ω the entire domain including the interior and exterior of the solid body. Note that we introduce the following scales for the non-dimensionalization: H for length, U_0 for velocity, H/U_0 for time and $\rho_f U_0^2$ for the pseudo-body force (ρ_f being the fluid density).

(i) Combined momentum equations

$$\frac{\partial \boldsymbol{u}}{\partial t} + \boldsymbol{u}\cdot\nabla\boldsymbol{u} = \frac{\eta_r \nabla^2 \boldsymbol{u}}{Re} - \nabla p + \frac{(1-\eta_r)\nabla\cdot\boldsymbol{B}}{ReWi} + \boldsymbol{\lambda} \quad \text{in } \Omega, \tag{2.1}$$

where $\boldsymbol{u}$ and p denote the fluid velocity and pressure, respectively; $\boldsymbol{\lambda}$ is the vectorial Lagrange multiplier (pseudo-body force); the Reynolds number is defined by $Re = \rho_f U_0 H/\eta_0$ (η_0 being the total zero-shear-rate viscosity of the fluid $\eta_0 = \eta_s + \eta_p$, and U_0 being the characteristic speed of a squirmer which will be defined later). Note that η_s and η_p are, respectively, the fluid solvent viscosity and polymer viscosity, and η_r denotes the ratio of the solvent viscosity (η_s) to the total zero-shear-rate viscosity of the fluid (η_0). Here, Wi is the Weissenberg number defined by $Wi = \lambda_t U_0/H$ (λ_t being the fluid relaxation time), and $\boldsymbol{B}$ is the polymer configuration tensor related to the polymer stress tensor $\boldsymbol{\tau}$ via $\boldsymbol{\tau} = \eta_p(\boldsymbol{B} - \boldsymbol{I})/\lambda_t$. The fluids in the solid domain satisfy the rigid-body motion constrain

$$\boldsymbol{u} = \boldsymbol{U} + \boldsymbol{\omega}_s \times \boldsymbol{r} + \boldsymbol{u}_s \quad \text{in } P_0, \tag{2.2}$$

$$(\rho_r - 1)V_s^* \frac{\mathrm{d}\boldsymbol{U}}{\mathrm{d}t} = -\int_{P_0} \boldsymbol{\lambda}\,\mathrm{d}\boldsymbol{x}, \tag{2.3}$$

$$(\rho_r - 1)\boldsymbol{J}^* \frac{\mathrm{d}\boldsymbol{\omega}_s}{\mathrm{d}t} = -\int_{P_0} \boldsymbol{r}\times\boldsymbol{\lambda}\,\mathrm{d}\boldsymbol{x}. \tag{2.4}$$

In (2.2)–(2.4), $\boldsymbol{r}$ is the position vector with respect to the mass centre of the particle; $\boldsymbol{U}$ and $\boldsymbol{\omega}_s$ are the particle translational velocity and angular velocity; $\boldsymbol{u}_s$ denotes the velocity distribution for the squirmer dynamics which we will introduce later; ρ_r is the particle–fluid density ratio, $\rho_r = \rho_s/\rho_f$, where here $\rho_r = 1$; V_p^* denotes the dimensionless particle volume defined by $V_p^* = V_p/H^3$ with V_p, being the particle volume, and $\boldsymbol{J}^*$ is the dimensionless moment of inertia defined by $\boldsymbol{J}^* = \boldsymbol{J}/\rho_s H^5$.

(ii) Continuity equation

$$\nabla\cdot\boldsymbol{u} = 0 \quad \text{in } \Omega. \tag{2.5}$$

(iii) On the viscoelastic fluid, the Giesekus constitutive equation is adopted here:

$$\frac{\partial \boldsymbol{B}}{\partial t} + \boldsymbol{u}\cdot\nabla\boldsymbol{B} - \boldsymbol{B}\cdot\nabla\boldsymbol{u} - (\nabla\boldsymbol{u})^{\mathrm{T}}\cdot\boldsymbol{B} + \frac{\alpha}{Wi}(\boldsymbol{B}-\boldsymbol{I})^2 + \frac{\boldsymbol{B}-\boldsymbol{I}}{Wi} = 0 \quad \text{in } \Omega. \tag{2.6}$$

In (2.6), α is the mobility parameter to quantify the shear-thinning effect (where $\alpha = 0$ gives the Oldroyd-B constitutive equation with constant viscosity). A fractional-step time scheme is employed to decouple system (2.1)–(2.6) into the fluid, particle and the viscoelastic subproblems. One can refer to the works of Yu & Shao (2007) and Yu *et al.* (2019) for more details on the discretization schemes. Significantly, it is challenging to overcome numerical instability or low accuracy of the results at high Wi. This requires us to ensure the symmetry and positive definiteness of the configuration tensor $\boldsymbol{B}$, and

to discretize the convection term with a high precision. Accordingly, we rewrite $\boldsymbol{B}$ and $\boldsymbol{u}$ in the form of the following components to obtain $\boldsymbol{B}^{n+1}$, $\boldsymbol{B} = \{b_{ij}\}_{i,j=1}^{3}$ with $b_{ij} = b_{ji}$ and $\boldsymbol{u} = \{u_i\}_{i=1}^{3}$. We employ the scheme proposed by Vaithianathan & Collins (2003) to solve (2.6); using the usual Cholesky analysis for a real symmetric and positive definite matrix, $\boldsymbol{B}$ can be decomposed into $\boldsymbol{B} = \boldsymbol{\Lambda} \cdot \boldsymbol{\Lambda}^T$, where $\boldsymbol{\Lambda} = \{l_{ij}\}_{i,j=1}^{3}$ is a lower triangular matrix ($l_{ij} = 0$ for $j > i$) with positive diagonal elements $l_{ii} > 0$. The solution of tensor $\boldsymbol{B}$ is hence transformed into solving tensor $\boldsymbol{\Lambda}$. We further adopt the exponential function to replace diagonal elements as $l_{ii} = \mathrm{e}^{\widetilde{l}_{ii}}$. Substituting the above relations into (2.6) yields a set of equations related to $\boldsymbol{\Lambda}$ (see Appendix A for details). Utilizing the updated $\boldsymbol{u}^{n+1}$, one can solve (A2)–(A3) explicitly. The convection term is discretized by the high precision MUSCL scheme (monotone upstream-centered scheme for conservation laws), and the fourth-order Runge–Kutta method is used for time integration.

In the spherical squirmer model, a progressive waving envelope is introduced to mimic both radial and angular oscillations on the boundary of a micro-swimmer with arrays of cilia like *Volvox* (Pedley *et al.* 2016). In the framework of the fictitious domain method, a given velocity distribution $\boldsymbol{u}_s$ (see (2.2)) is exerted at the spherical solid domain to realize the self-propulsion of the body (squirmer). This velocity is performed with the following divergence-free velocity field (in the frame of reference moving with the body) inside the squirmer (Li *et al.* 2016; Lin & Gao 2019; More & Ardekani 2020; Ouyang *et al.* 2022):

$$\boldsymbol{u}_s = \left[\left(\frac{r}{a}\right)^m - \left(\frac{r}{a}\right)^{m+1}\right]\left(u_\theta^s \cot\theta + \frac{\mathrm{d}u_\theta^s}{\mathrm{d}\theta}\right)\boldsymbol{e}_r + \left[(m+3)\left(\frac{r}{a}\right)^{m+1} - (m+2)\left(\frac{r}{a}\right)^m\right]u_\theta^s \boldsymbol{e}_\theta, \tag{2.7}$$

where a is the radius of the squirmer, r is the distance from the squirmer's centre, $\boldsymbol{e}_r$ and $\boldsymbol{e}_\theta$ are, respectively, the unit vectors along the radial and polar directions, m is an arbitrary positive integer and $m = 5$ is adopted here; u_θ^s is expressed as

$$u_\theta^{\mathrm{s}}(\theta) = B_1 \sin\theta + B_2 \sin\theta\cos\theta, \tag{2.8}$$

where θ is the angle concerning the swimming direction, and B_1 and B_2 are the swimming parameters. The mode of the squirmer can be defined as a puller ($\beta > 0$, e.g. *Chlamydomonas*), pusher ($\beta < 0$, e.g. *Escherichia coli*) or neutral squirmer ($\beta = 0$), based on the value of $\beta = B_2/B_1$ ($B_1 > 0$) (Ishikawa & Pedley 2008). In the Stokes flow regime, the velocity of a squirmer in an infinite domain is $U_0 = 2B_1/3$ (Lighthill 1952), and we adopt it as the velocity scale in this study.

Similarly, we define a squirmer dumbbell with two identical squirmers arranged in tandem, assuming that a rigid rod connecting the two identical squirmers is a phantom, and the two squirmers can only rotate around the mass centre O, as shown in figure 1. Here, d_{s} is the distance between the centre of mass of each squirmer and therefore $d_s \geq 2a$. $d_s = 2a$ indicates that the two bodies touch each other, and this distance is adopted here if not otherwise specified. The periodic boundary conditions (the black dotted lines) are employed at all the boundaries to simulate the infinite flow field, defined as

$$f(x, t) = f(x + K, t), \tag{2.9}$$

where $f(x)$ denotes the any physical quantity, and K is the period length of the flow field ($K = W$, R and L along the x, y and z axes, respectively). The motion of a squirmer or squirmer dumbbell is governed by (2.3) and (2.4). For the details of the squirmer dynamics employing the DF-FDM, one can refer to the work of Lin & Gao (2019) and Ouyang *et al.* (2022).

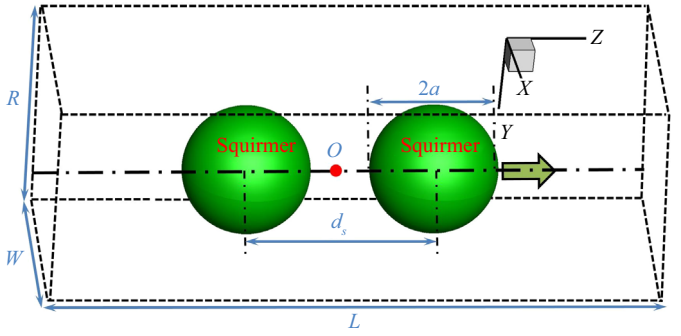

Figure 1. Schematic of a squirmer dumbbell swimming in an infinite flow (the blue arrow indicates the swimming direction).

3. Validation of a squirmer through Giesekus fluids

Our DF-FDM has been shown to be accurate in dealing with the swimming of a squirmer in a Newtonian fluid at $Re = 0$ (Lin & Gao 2019) and at finite Re (Ouyang *et al.* 2022) when compared with the available theoretical solution and the numerical results. In this section, we further conduct a validation of a squirmer swimming in Giesekus viscoelastic fluids. Here, the calculation parameters are set to be coincident with the work of Li, Karimi & Ardekani (2014). The computational domain is adopted with $R \times W \times L = [-16a, 16a] \times [-16a, 16a] \times [-16a, 16a]$. Hence, the origin of the coordinate system is located at the centre of the domain. These dimensions have shown to be convergent when calculating the locomotion of a squirmer carrying a spherical cargo (Ouyang *et al.* 2023). The swimming Reynolds is set to $Re = 0.01$ at which the effects of the inertia on the swimming speed can be neglected (Wang & Ardekani 2012). On the viscoelastic fluids, the viscosity ratio $\eta_r = 0.5$ and mobility factor $\alpha = 0.2$ are employed, if not otherwise specified. A squirmer is initially released at the centre of the domain with its orientation directing along the z-axis, and its velocity reaches a steady state after the initial transient dynamics. The moving mesh technology, shifting the flow field and the body position one mesh distance once the body moves a horizontal position that is greater than the centre of the domain in the horizontal direction (z-axis), is employed to keep the squirmer nearly at the centre of the calculated domain for better plotting of the flow fields (maintaining the squirmer at the centre of the flow field). Note that the squirmer's translation and rotation along the x- and y-axes are restricted for better comparison of the speeds if not otherwise specified. A mesh size of $32\Delta x$ across the diameter of a squirmer and a time step $\Delta t = 5 \times 10^{-4}$, shown to be convergent (Lin & Gao 2019), are adopted in this study. Figure 2 presents the steady swimming speed of the squirmer with Weissenberg number (Wi), showing that our results agree well with these of Zhu *et al.* (2012) and Li *et al.* (2014).

4. Results and discussion

A squirmer and a squirmer dumbbell through a Giesekus fluid is simulated in this section with the swimming Reynolds number and Weissenberg number, respectively, in the ranges of $5 \leq Re \leq 100$ and $1 \leq Wi \leq 12$. Note that the squirmer's radius a is adopted as the characteristic length, hence the Weissenberg number here is defined as $Wi = \lambda_t U_0/a$. The calculation parameters in § 3 are adopted if not otherwise specified. In the following subsections, we first consider how fluid inertia and elasticity jointly affect the swimming of a squirmer. Subsequently, we investigate the hydrodynamics between the two assembled

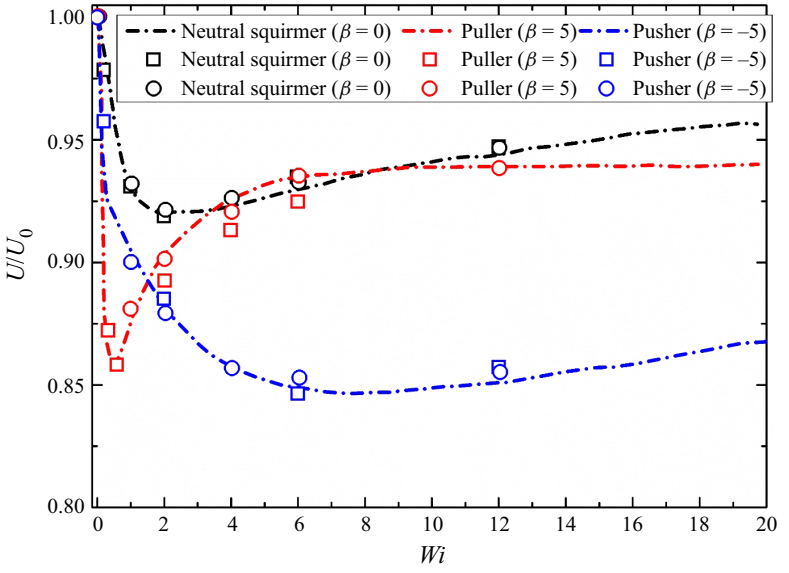

Figure 2. Steady swimming speed of a squirmer with Wi ($Re = 0.01$). The velocity is normalized with the steady speed of the squirmer in Stokes flow, i.e. $U_0 = 2B_1/3$. The dashed lines denote the results of Zhu *et al.* (2012); the squares denote the results of Li *et al.* (2014); the circles denote the present results.

squirmers, expecting to find a faster squirmer dumbbell. We also discuss the hydrodynamic force contribution in driving the squirmer (dumbbell), their energy expenditure and hydrodynamic efficiency.

4.1. *Fluid elasticity speeds up an inertial neutral squirmer*

The steady swimming speed of an inertial squirmer through a Giesekus fluid is presented in figure 3. The main finding in this section is that the speed of the neutral squirmer in viscoelastic fluids ($Wi = 2$) increases monotonically with Re (see figure 3*a*), in contrast to that of the neutral squirmer ($\beta = 0$) through a Newtonian fluid (holding U_0 constant with Re (Chisholm *et al.* 2016)). Its speed increases by approximately 26% from $Re = 0.01$ to 100. Figure 4(*a*,*b*) presents the velocity magnitudes around the neutral squirmer. It is seen that the velocity gradient in front of (near the boundaries) the neutral squirmer is more significant at $Re = 100$ than it is at $Re = 0.01$, indicating a faster velocity decay for $Re = 100$. This pattern agrees with the conclusion that a more rapid decay leads to a better efficiency (Leshansky 2009). Note that the velocity is normalized with U_0. Recalling that a squirmer with different self-propelled modes (depending on β) displays divergent speeds with finite fluid inertia (Li *et al.* 2016), this leads to the conclusion that, with increasing Re, a puller 'pulls' the vorticity (generated by the puller) to accumulate around the body, hence hindering its speed, whereas a pusher 'pushes' the vorticity (generated by the pusher) downstream, hence speeding it up. Regarding our results for the pusher and puller, as shown in figure 3(*a*), a similar pattern is obtained. To exclude the effect of fluid inertia on the speed, we simulate the squirmers swimming in a Newtonian fluid at $Re = 50$. The pusher with $\beta = -1$ swims slightly slower in a Newtonian fluid (1.48, not shown in figure 3*a*) than in Giesekus fluids (1.49, $Wi = 2$). In contrast, the counterpart puller with $\beta = 1$ has a faster speed in a Newtonian fluid (1.05, not shown in figure 3*a*) than in Giesekus fluids (0.99, $Wi = 2$). This may be explained by analysing the vorticity

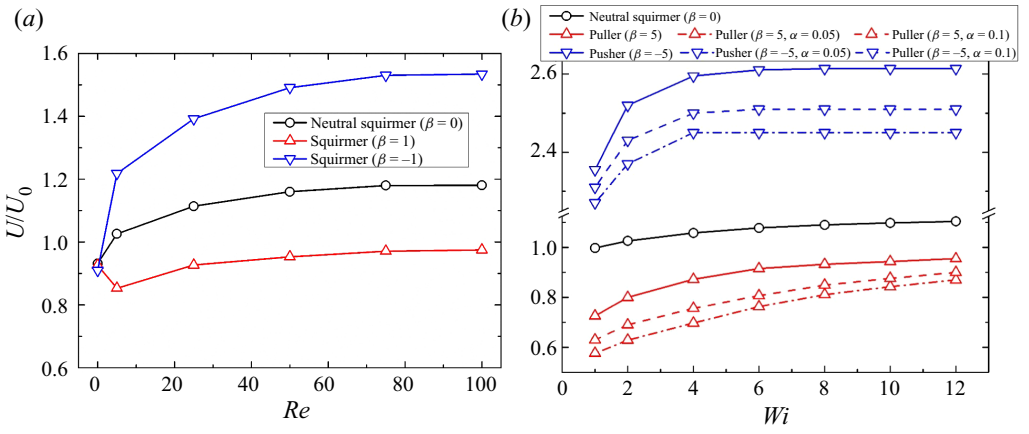

Figure 3. Steady swimming speed of an inertial squirmer through a Giesekus fluid. (*a*) Speed variation with Re ($Wi = 2$); (*b*) speed variation with Wi ($Re = 5$). The curves without annotation indicate $\alpha = 0.2$.

distribution around the puller, as shown in figure 4(*c*,*d*). A Newtonian fluid contributes to a better convection of the vorticity than a Giesekus fluid (a slightly more stretched vortex at the rear of the body is observed in a Newtonian fluid), and hence it reduces the vorticity (it hinders the speed) accumulated around the body.

The second finding in this section is that the speed of the finite inertial squirmer increases monotonically with Wi ($Wi \geq 1$), as shown in figure 3(*b*). This tendency of the speeds with Wi holds when changing α. However, a greater α yields a faster speed for the pusher and puller. This pattern is similar to the result that the speed of a neutral squirmer ($\beta = 0$) increases with α at a relatively high Wi ($Wi = 3$) (Binagia *et al.* 2020). Figure 5 presents the velocity magnitudes around the squirmers at $Re = 5$. As the fluid stresses generated in the extensional flow at the rear of the squirmer drive the flows toward the body (Zhu *et al.* 2011), the extended wakes and a region with slower decay of the velocity are observed. A higher Wi yields a more extensive extended wake, in agreement with the result of a squirmer swimming in viscoelastic fluids at $Re = 0$ (Zhu *et al.* 2011). At $Re = 0$, the fluid elasticity contributes to the divergent speeds for a pusher and a puller with increasing Wi (see figure 2). Zhu *et al.* (2012) have reported that the squirmer induces flows which yield increasing elongational viscosities with Wi (served as an additional elastic force), possibly positive or negative (based on the swimming modes), of the locomotion. The inclusion of fluid inertia ($Re = 5$) here breaks this pattern, and the vorticity around the squirmers may provide insight into understanding the mechanism. As shown in figure 6, increasing Wi results in better convection of the vorticity downstream (the vorticity around the squirmers expands more transversely with $Wi = 1$ than $Wi = 12$), hence speeding up the puller and pusher. This indicates the fluid inertia's dominance in affecting the swimming of the squirmer here.

4.2. *Pusher–puller dumbbell swims faster than other assemblies*

This section further investigates the squirmer dumbbell swimming in a Giesekus fluid. Here, we consider two identical and two different squirmers in assembling the dumbbell for completeness. The main finding in this section is that the pusher–puller (the puller is in front of the pusher) dumbbell swims significantly faster than other dumbbells, as shown in figure 7. For example, its speed is approximately 190% faster than that of the

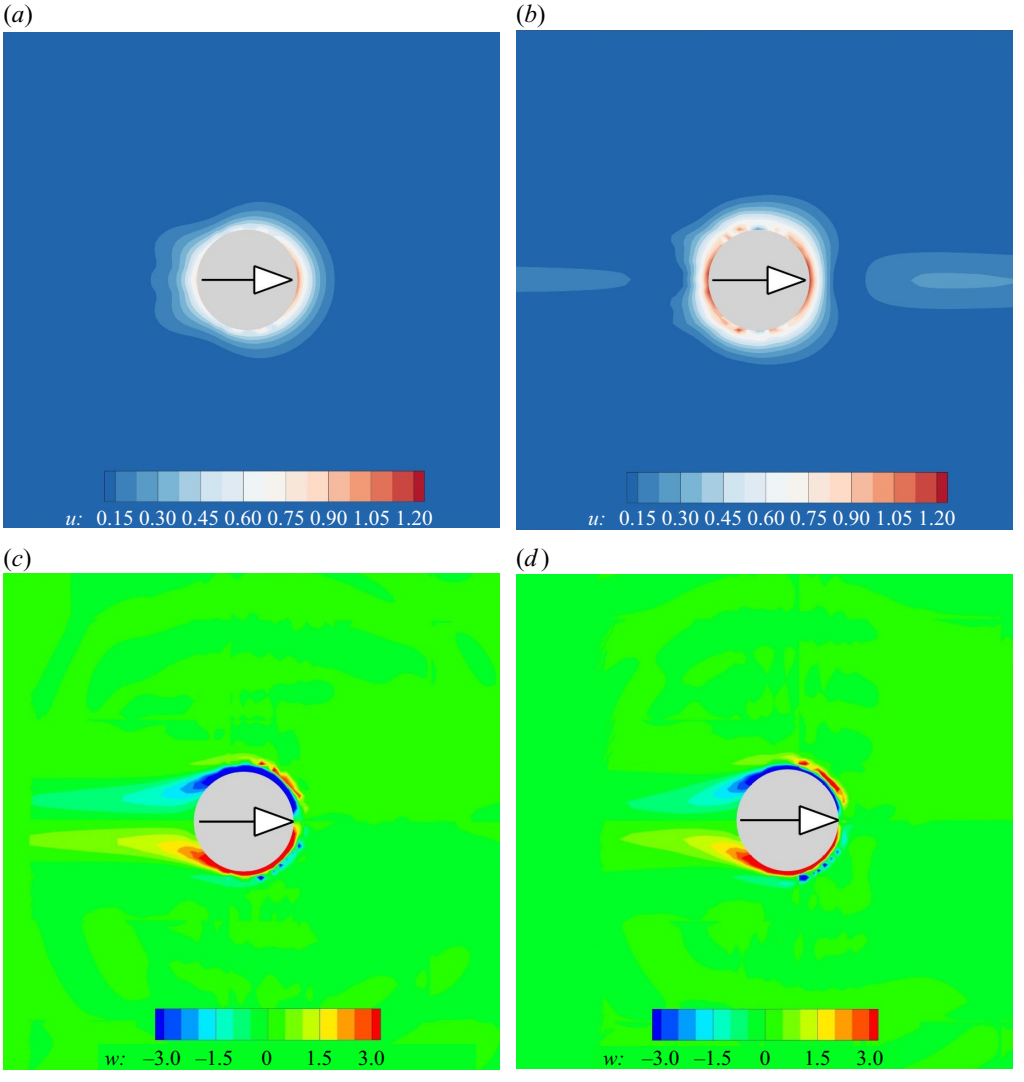

Figure 4. Velocity magnitudes and vorticity contours around the squirmers. (*a*) Velocity magnitudes for the neutral squirmer ($\beta = 0$) at $Re = 0.01$ and $Wi = 2$; (*b*) velocity magnitudes for the neutral squirmer ($\beta = 0$) at $Re = 100$ and $Wi = 2$; (*c*) vorticity contours for a puller ($\beta = 1$) with $Re = 50$ in a Newtonian fluid; (*d*) vorticity contours for a puller ($\beta = 1$) with $Re = 50$ at $Wi = 2$.

puller–pusher (the pusher is in front of the puller) at $Re = 0.01$ and $Wi = 12$. The velocity magnitude around the dumbbells may provide insight into understanding the physics, as shown in figure 8. Comparing figures 8(*c*) and 8(*d*), it is seen that the velocity magnitude of the puller–pusher dumbbell is more fore-and-aft symmetric than that of pusher–puller one. For the viscoelastic fluid in the Stokes flow regime, breaking the symmetry of flows around the body is the crucial hydrodynamics for self-propulsion (Pak *et al.* 2012). Hence, the pusher–puller dumbbell uses the hydrodynamic force in self-propulsion better than the puller–pusher one. Meanwhile, the velocity gradient in front of the pusher–puller dumbbell is more significant than that of the puller–pusher one, corresponding to the fact that a more rapid decay yields a faster speed, as mentioned in the above section. For the puller

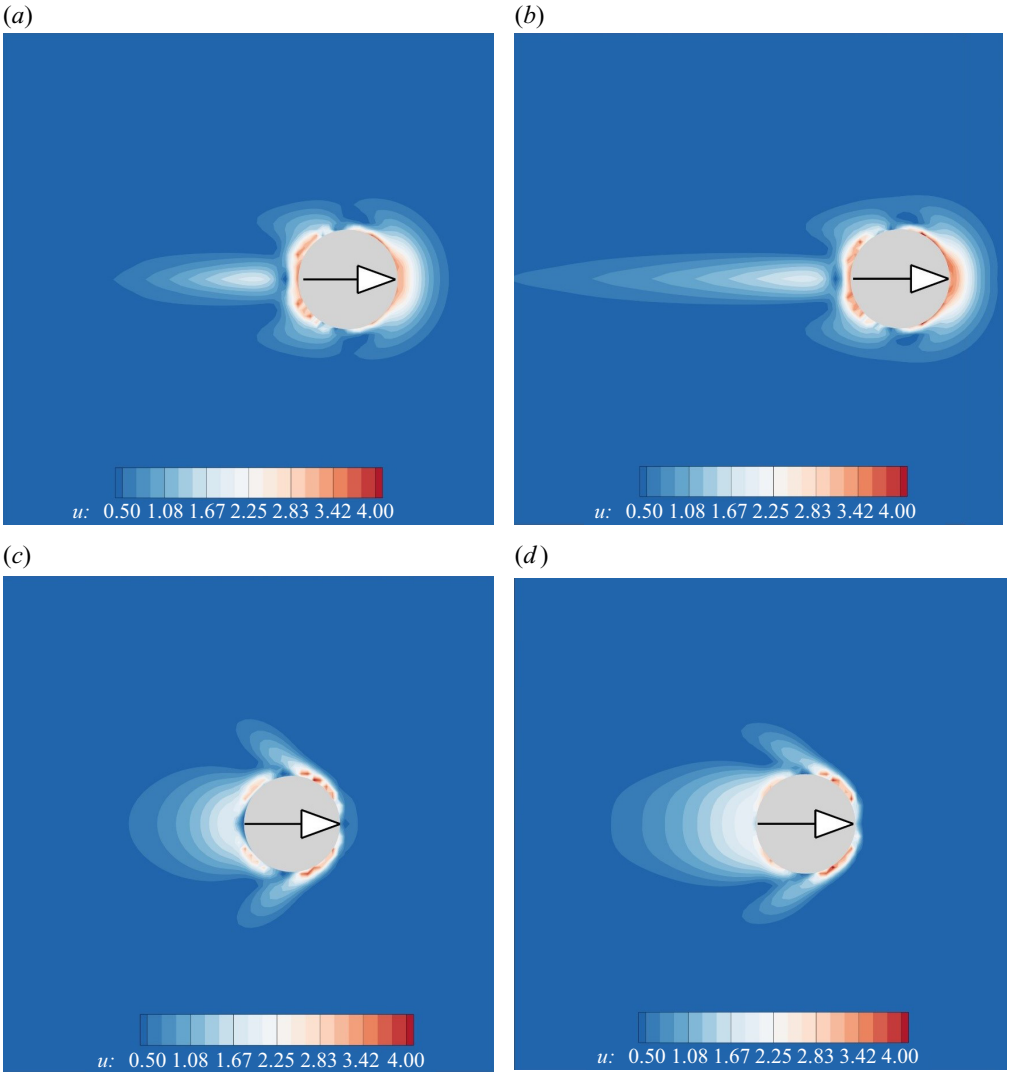

Figure 5. Comparing the velocity magnitudes around the squirmers at $Re = 5$. (*a*) Pusher ($\beta = -5$) at $Wi = 1$; (*b*) pusher ($\beta = -5$) at $Wi = 12$; (*c*) puller ($\beta = 5$) at $Wi = 1$; (*d*) puller ($\beta = 5$) at $Wi = 12$. The velocity magnitude is normalized with $2B_1/3$.

and pusher dumbbells (see figure 8*a*,*b*), their velocity magnitudes show a slightly reversed longitudinally (in the swimming direction). It is difficult for this discrepancy to provide an intuitive hydrodynamic mechanism in understanding their different speeds at $Wi = 12$ (see figure 7). However, the pattern of our results for the squirmer dumbbells (the assembled two identical pullers, pushers or neutral squirmers) is in good agreement with that of an individual squirmer swimming through a Giesekus fluid, especially at $Wi \geq 6$ (compared with figure 2). Zhu *et al.* (2012) have reported that the region of stretched polymers behind the swimmer becomes thinner and the induced elastic resistance decreases with Wi, thus explaining the slow recovery of the swimming speed with increasing Wi ($Wi \geq 6$). However, due to the different swimming modes for these three squirmer dumbbells, it is subtle to quantitatively indicate the recovery ratios by analysing the induced fluid fields.

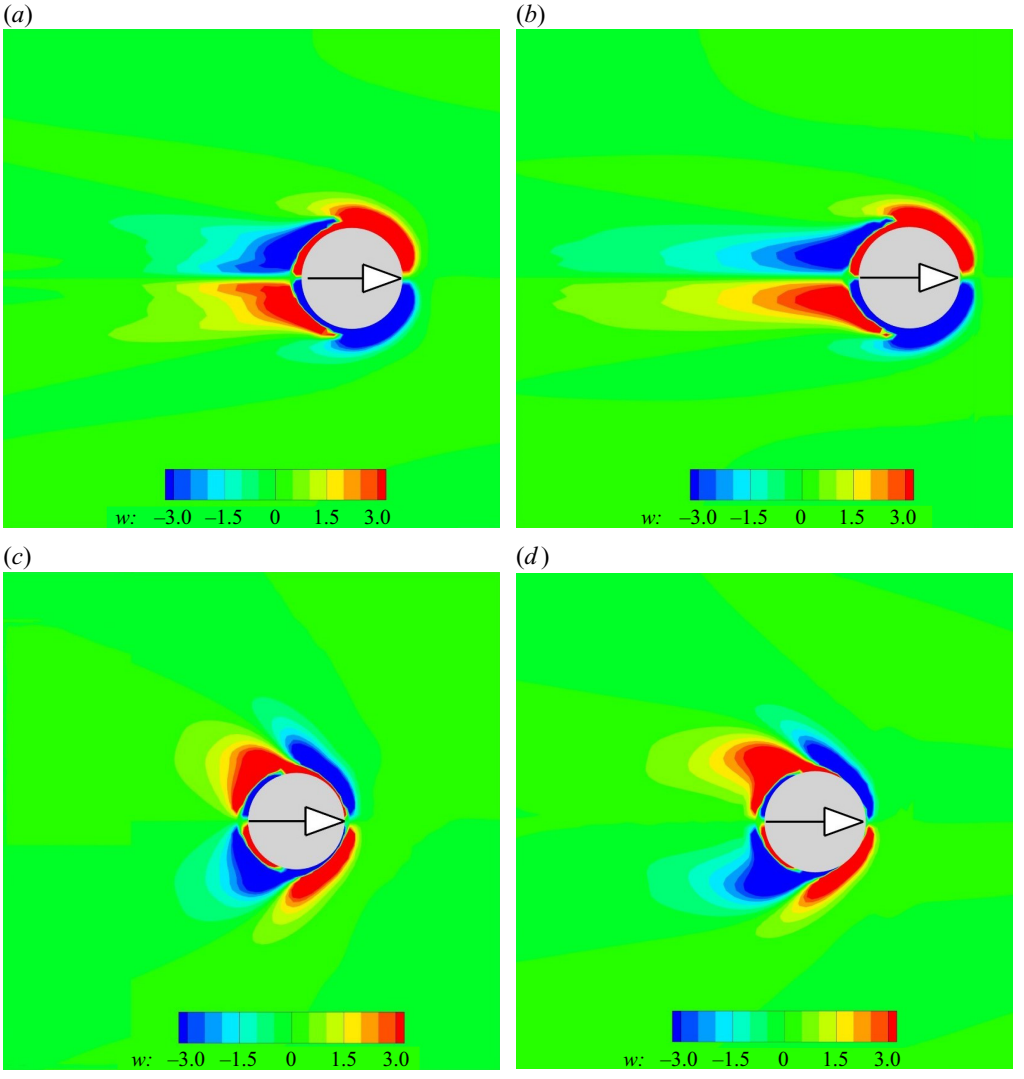

Figure 6. Comparing the vorticity around the squirmers at $Re = 5$. (*a*) Pusher ($\beta = -5$) at $Wi = 1$; (*b*) pusher ($\beta = -5$) at $Wi = 12$; (*c*) puller ($\beta = 5$) at $Wi = 1$; (*d*) puller ($\beta = 5$) at $Wi = 12$.

We further plot the velocity contours of the puller–pusher (figure 8*e*) and pusher–puller (figure 8*f*) on the z-axis. Focusing on the areas at the front and rear of the puller–pusher, we find a greater velocity behind the body than that at its front. As a greater velocity yields a lower pressure, the front and rear pressure difference induces a net pressure opposite to the swimming direction. On the contrary, the pusher–puller induces a net pressure in the swimming direction (see figure 8*f*, the velocity in front of the pusher–puller is greater than that in its rear). This indicates the possible mechanism for our finding that the pusher–puller swims much faster than the puller–pusher.

To further illustrate the possible hydrodynamic mechanism for the faster pusher–puller dumbbell, we plot the schematic shown in figure 9. The swimming of the dumbbells is determined by the flows induced around the bodies. An individual puller (pusher) 'pulls' (pushes) the flows to achieve self-propulsion (Li *et al.* 2016; More & Ardekani 2020;

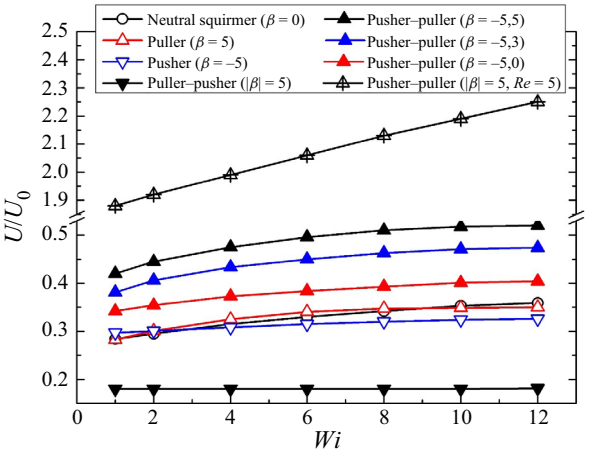

Figure 7. Steady swimming speed of squirmer and squirmer dumbbells through a Giesekus fluid with Wi (the unmarked curves (Re) indicate $Re = 0.01$).

Ouyang *et al.* 2022), and the assembled dumbbells generate the superimposed flows (see figure 9, the green and blue arrows) induced by the individual squirmers. Since the bigger green and blue arrows in the front or at the rear of the dumbbells are only partly exerted on the sides of the bodies, the smaller green and blue arrows (the dominant role) in the middle of the bodies may help in understanding the driving effects. Note that the smaller arrows in the middle of the bodies indicate the hindrance of the hydrodynamic interactions between the individual squirmers. We find that the pusher–puller induces the superimposed positive driving effect (see figure 9*c*), in contrast to the puller–pusher, which induces the superimposed negative driving effect (see figure 9*d*). This results in the fastest pusher–puller and the slowest puller–pusher. Additionally, the middle smaller arrows for puller–puller and pusher–pusher are cancelled (see figure 9*a*,*b*), hence their speeds are between the pusher–puller and puller–pusher. However, it is challenging for this schematic to indicate the mechanism of the different speeds between the pusher–pusher and puller–puller.

We further focus on the pusher–puller dumbbells to elaborate on essential factors affecting their speed in the viscoelastic fluids. Maintaining the pusher with $\beta = -5$, as shown in figure 7, the decrease of the puller (from $\beta = 5$ to 3) yields a lower speed, and this pattern applies down to $\beta = 0$ (neutral squirmer). This indicates that the front-arranged puller has a positive effect on driving the dumbbell. The speed of the pusher–pullers increases with Re, displaying a similar pattern to that of the individual pusher. Our results also emphasize that, even at a finite but small Reynold number ($Re = 5$), the fluid inertia rather than the elasticity dominates the pusher–puller (the swimming speed enhances significantly from $Re = 0.01$ to 5).

4.3. *Force contribution analysis*

To better understand the possible mechanism for the above results, we examine the force contribution of the squirmers (dumbbells). For a steady swimming squirmer (dumbbell) through a Giesekus fluid, the net force on the body can be decomposed into pressure, viscous and polymeric contributions (force free); in the swimming direction (z-axis), it is $F_z = F_z^{pres} + F_z^{visc} + F_z^{poly} = 0$. The pressure force, the viscous force and the polymeric

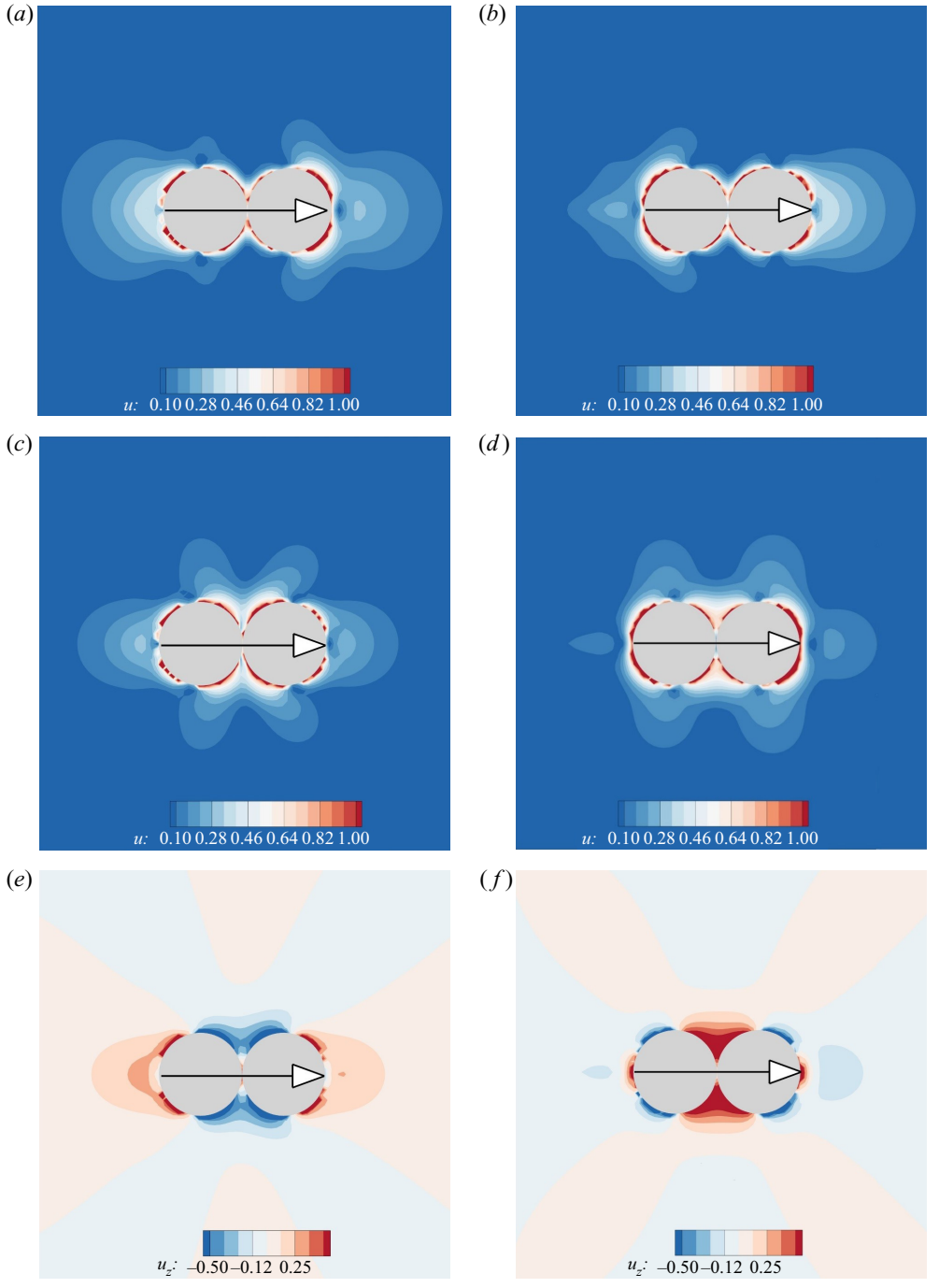

Figure 8. Comparing the velocity magnitudes around the squirmer dumbbells at $Re = 0.01$ and $Wi = 12$. (*a*) Puller–puller ($\beta = 5$); (*b*) pusher–pusher ($\beta = -5$); (*c*) puller–pusher ($\beta = 5$, $\beta = -5$); (*d*) pusher–puller ($\beta = -5$, $\beta = 5$); (*e*) and (*f*), respectively, denote the velocity contours of (*c*) and (*d*) on the z-axis. The velocity magnitude is normalized with $2B_1/3$.

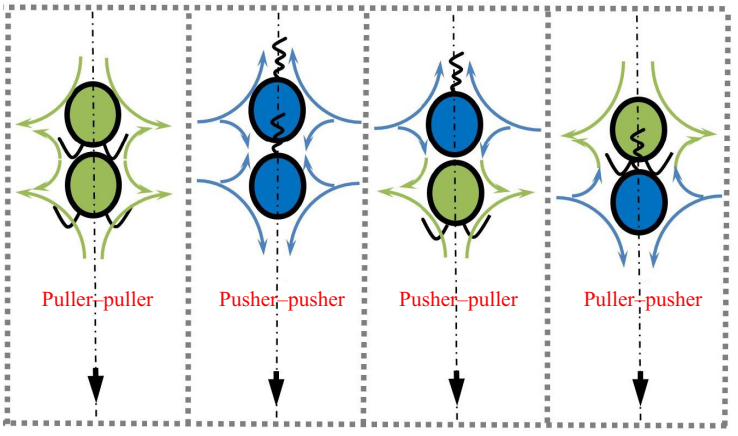

Figure 9. Schematic to compare the swimming mechanisms between the squirmer dumbbells in an infinite fluid field. (*a*) Puller–puller dumbbell; (*b*) pusher–pusher dumbbell; (*c*) pusher–puller dumbbell; (*d*) puller–pusher dumbbell. The green and blue swimmers, respectively, denote the puller and the pusher, and the arrows correspond their induced flows. The dashed boundary lines represent the periodic conditions, and the black arrows indicate the swimming direction.

force have the following forms:

$$F_z^{pres} = -\int_{\partial P_0} n_z p \, \mathrm{d}S, \tag{4.1}$$

$$F_z^{visc} = \eta_s \int_{\partial P_0} \left[2n_z \frac{\partial u_z}{\partial z} + n_x \left(\frac{\partial u_z}{\partial x} + \frac{\partial u_x}{\partial z} \right) + n_y \left(\frac{\partial u_z}{\partial y} + \frac{\partial u_y}{\partial z} \right) \right] \mathrm{d}S, \tag{4.2}$$

$$F_z^{poly} = \int_{\partial P_0} [n_z \tau_{zz} + n_y \tau_{yz} + n_x \tau_{xz}] \, \mathrm{d}S, \tag{4.3}$$

where η_s denotes the viscosity of the fluid, $\boldsymbol{n}$ is the unit normal outward the surface S of the body. In (4.3), the polymer force can be further decomposed into the normal polymeric force, F_{zn}^{poly}, and the polymeric shear force, F_{zs}^{poly}

$$F_{zn}^{poly} = \int_{\partial P_0} n_z \tau_{zz} \, \mathrm{d}S, \tag{4.4}$$

$$F_{zs}^{poly} = \int_{\partial P_0} [n_y \tau_{yz} + n_x \tau_{xz}] \, \mathrm{d}S. \tag{4.5}$$

Figure 10 presents the force contributions for a squirmer swimming in a Giesekus fluid, in which the forces are normalized by $\eta_0 U_0 a$. Regarding a neutral squirmer across Re, the viscous force F_z^{visc} increases monotonically, but the total polymeric force F_z^{poly} almost maintains an unchanged and negative contribution (see figure 10*a*). This indicates that the increase of the fluid inertia mainly results in the competition between the pressure (not shown) and the viscous force by altering the flows around the body. Meanwhile, F_z^{visc} is dominant in driving (positive contribution) the squirmer, similar to the results of Binagia *et al.* (2020). However, F_{zn}^{poly} makes a more considerable negative contribution than F_{zs}^{poly}, in contrast to the results of Binagia *et al.* (2020). This may be because we consider finite fluid inertia here ($Re = 5$), but the reference adopts swimming that falls into the Stokes flow regime ($Re = 0$). With fluid inertia, the flows around the body tend to become

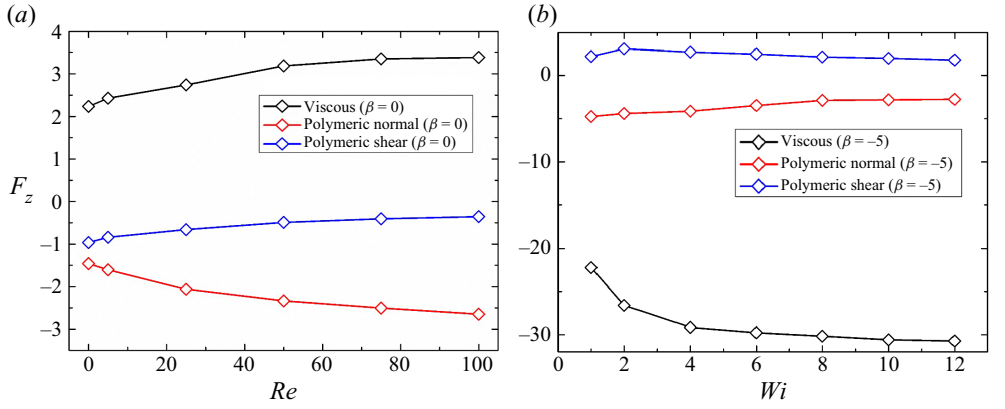

Figure 10. Force contribution of a squirmer through a Giesekus fluid. (*a*) Forces with Re ($Wi = 2$); (*b*) forces with Wi ($Re = 5$).

fore-and-aft asymmetric. This rearranges the distribution and hence the contribution of F_{zn}^{poly}. For a pusher ($\beta = -5$) across Wi (see figure 10*b*), we find the total polymeric force F_z^{poly} holds (positive contribution), but F_z^{visc} decreases monotonically (negative contribution) and converges to approximately 31 at $Wi = 12$. This result is different from the speed of a neutral squirmer ($Re = 0$) through Giesekus fluids (Binagia *et al.* 2020) where the shear polymer force makes a negative contribution. This may be because of the different self-propelling modes and the hydrodynamics (here, we consider a pusher with the finite fluid inertia ($Re = 5$)). The pattern of F_z^{visc} with Wi also indicates the balance of energy dissipation into the fluids, and the convergent viscous force may indicate a convergent speed, as shown in figure 3. Figure 11 presents the component of the polymer stress $\boldsymbol{\tau}_{zz}$ distributed around the squirmer. A larger amount of extensional stress in the neutral squirmer's ($\beta = 0$) wake is observed at $Re = 100$ than at $Re = 5$ (see figure 11*a*,*b*). This may be because the fluid inertia contributes to the stretching of the wake. For the viscoelastic fluid, the isotropic polymer stress can be regarded as a 'pressure' (Yu *et al.* 2019). We infer that a larger $\boldsymbol{\tau}_{zz}$ around the rear of the squirmer generates a more significant elasticity-induced force in speeding up the body (along the z-axis). Considering the different self-propelling modes, we find that the pusher induces a more significant $\boldsymbol{\tau}_{zz}$ at the rear of the body than a neutral squirmer (see figure 11*a*,*c*). Moreover, a distinct $\boldsymbol{\tau}_{zz}$ is also observed at the pusher's sides and front, indicating that the 'push' effect results in deforming of the fluids around the body. With the increase of fluid elasticity (increasing Wi up to 12, see figure 11*d*), $\boldsymbol{\tau}_{zz}$ around the body becomes weaker. This high elasticity of the fluids resists the deforming flows induced by the slip velocity for driving the body, resulting in a somewhat converged swimming speed with Wi (see figure 3*b*, the pusher).

The force contribution of the squirmer dumbbell through a Giesekus fluid is presented in figure 12. The viscous force F_z^{visc} decreases monotonically with Wi, indicating the gradually increasing ratio of the total polymeric force. Swimming in the fluid with low elasticity (e.g. $Wi = 1$), the viscous force is dominant in driving (positive contribution) the dumbbells. Hence, it can be inferred that the velocity gradient around the dumbbells tends to be fore-and-aft asymmetric based on (4.2). The increase of Wi may induce the strong elastic wake, altering the distribution of the velocity gradient and weakening the viscous force. It can be concluded from figure 12 that the effect of the total polymeric force F_z^{poly} ($F_{zn}^{poly} + F_{zs}^{poly}$) is generally weaker than the viscous force. This indicates that

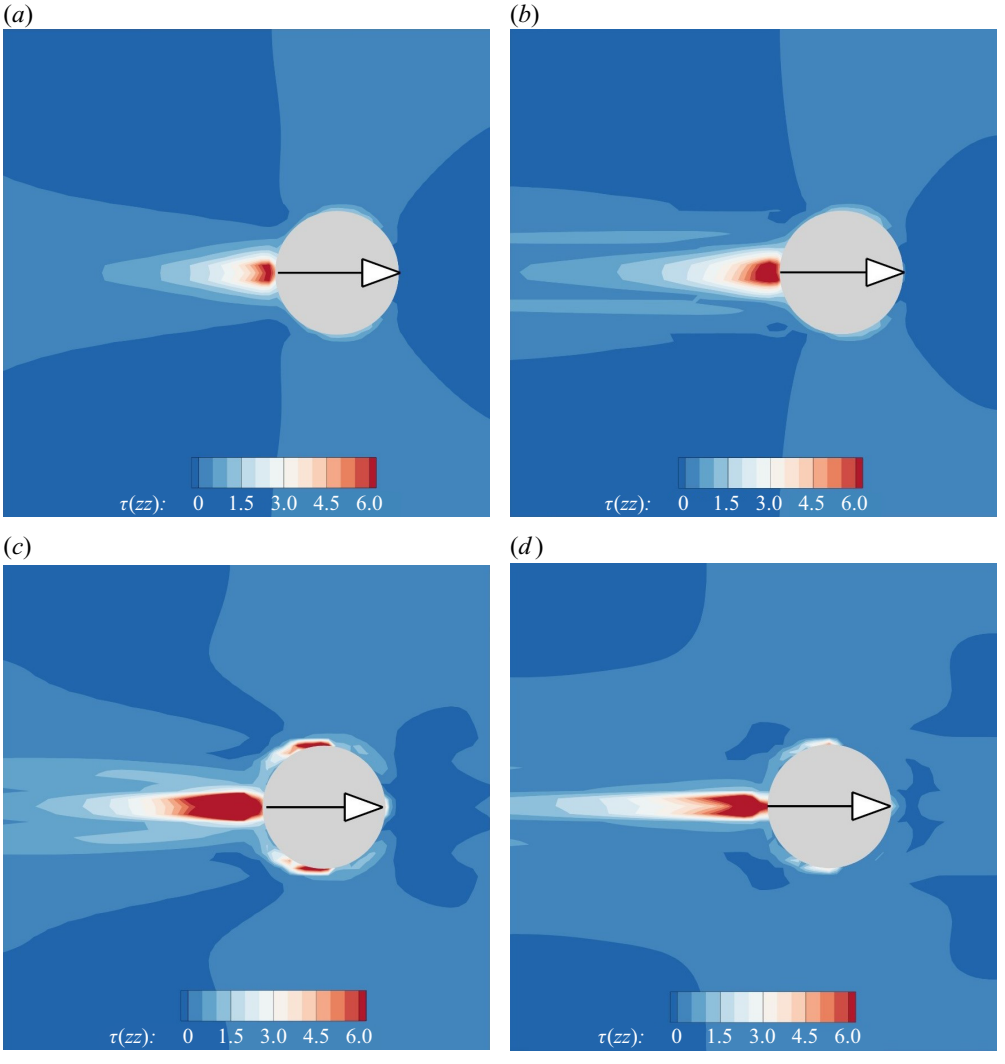

Figure 11. Component of polymer stress $\boldsymbol{\tau}_{zz}$ distribution around the squirmer. (*a*) $Wi = 2$, $\beta = 0$, $Re = 5$; (*b*) $Wi = 2$, $\beta = 0$, $Re = 100$; (*c*) $Wi = 2$, $\beta = -5$, $Re = 5$; (*d*) $Wi = 12$, $\beta = -5$, $Re = 5$.

the inclusion of fluid elasticity is not essential for the different swimming speeds between the pusher–puller and the puller–pusher, and the method of assembly may determine if they can effectively utilize the hydrodynamics for driving or not.

4.4. *Energy expenditure and hydrodynamic efficiency*

For a squirmer or squirmer dumbbell swimming through the fluids, the rate of work P can be written as

$$P = -\int_{\partial P_0} (\boldsymbol{u} \cdot \boldsymbol{\sigma}) \cdot \boldsymbol{n} \, \mathrm{d}S, \tag{4.6}$$

where $\boldsymbol{n}$ is the unit normal outward the surface S of the swimmer, and $\boldsymbol{\sigma}$ denotes the total stress tensor. Figure 13 presents the energy expenditure for the steady swimming of

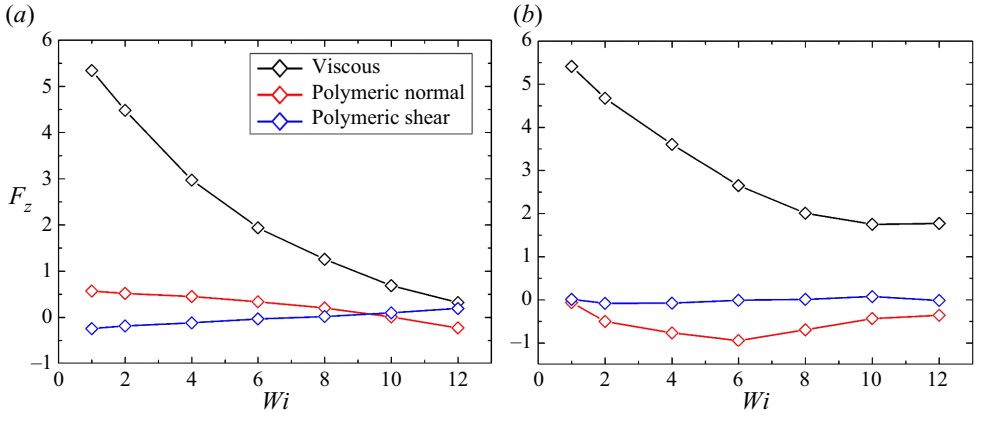

Figure 12. Force contribution of a squirmer dumbbell through a Giesekus fluid with Wi ($Re = 0.01$). (a) Pusher–puller ($|\beta| = 5$); (b) puller–pusher ($|\beta| = 5$).

a squirmer and squirmer dumbbell through a Giesekus fluid, in which P is normalized with P_N (P_N is defined as the power at a Newtonian ($Wi = 0$) fluid for the squirmer (dumbbell) with the same gait). Swimming in viscoelastic fluids ($Wi = 2$), as shown in figure 12(a), expends less energy than its Newtonian counterpart. This pattern is similar to that of a neutral squirmer ($\beta = 0$) swimming through viscoelastic fluids at $Re = 0$ (Binagia *et al.* 2020). The fluid inertia results in a decrease of energy expenditure, and the neutral squirmer maintains a larger P than that of the pusher or puller. At the finite $Re = 5$, as shown in figure 12(b), the normalized P decreases monotonically with Wi, in agreement with the pattern of a squirmer swimming at $Re = 0$ (Binagia *et al.* 2020). Meanwhile, it is seen that the energy expenditure is relevant with the steady swimming speeds, in which the faster counterpart squirmer (dumbbell) expends less energy. We further consider the hydrodynamic efficiency $\eta = P^*/P$, as shown in figure 14, in which P^* denotes the power necessary to move the swimmer at its swimming speed U. Note that P^* is obtained numerically. For viscoelastic fluids ($Wi = 2$, see figure 14a), η of the squirmer increases monotonically with Re. This pattern is also reported for the swimming of a squirmer in a Newtonian fluid. However, here we observe the divergent results with Re (in a Newtonian fluid, η of a counterpart squirmer presents only a perceptible difference up to $Re = 100$ (Chisholm *et al.* 2016)). Figure 14(b) presents η of an inertial squirmer (dumbbell) swimming through viscoelastic fluids ($Re = 5$). It is seen that η displays a positive relationship with the swimming speed of the counterpart swimmers, and the increase of Wi results in the increase of η. This result reproduces the conclusion that the elasticity of the fluid contributes to the enhancement of swimming efficiency (Zhu *et al.* 2012; Binagia *et al.* 2020), and this is regardless of fluid inertia.

5. Conclusion

We have studied the hydrodynamics of a spherical and a dumbbell-shaped squirmer in a Giesekus fluid. By systematically considering the swimmers' speed, energy expenditure and hydrodynamic efficiency, we attempt to shed light on how the fluid inertia and elasticity jointly affect their hydrodynamic behaviours. Our results indicate that, for the neutral squirmer, its speed increases monotonically with increasing Reynolds number in a Giesekus fluid, in contrast to holding a constant speed in a Newtonian one.

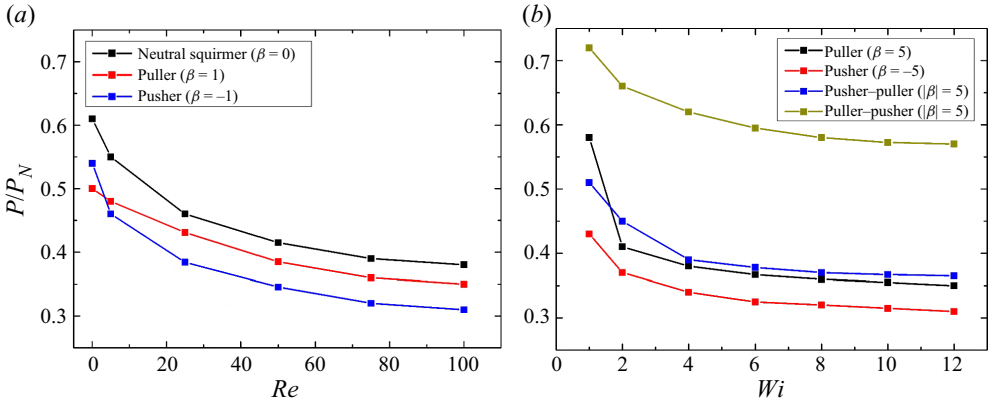

Figure 13. Energy expenditure for the steady swimming of a squirmer and squirmer dumbbell through a Giesekus fluid: (*a*) $Wi = 2$; (*b*) $Re = 5$.

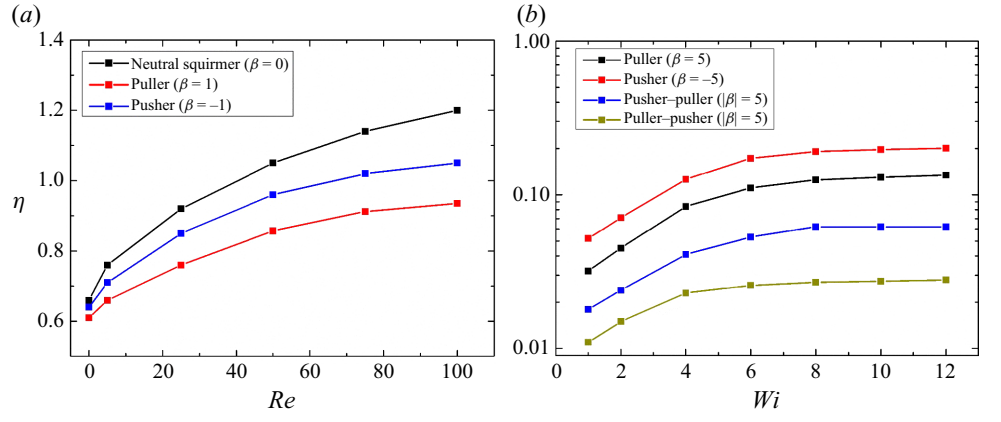

Figure 14. Hydrodynamic efficiency for the steady swimming of a squirmer and squirmer dumbbell through a Giesekus fluid: (*a*) $Wi = 2$; (*b*) $Re = 5$.

Meanwhile, the speed of the finite inertial squirmer increases monotonically with *Wi*. This may be due to the different fluid stresses generated in the extensional flow at the rear of the squirmer. Specifically, the increasing *Wi* results in better convection of the vorticity downstream, subsequently speeding up the puller and pusher.

Regarding the dumbbell squirmer, it is found that the pusher–puller dumbbell swims significantly faster than other dumbbells. For example, its speed can be approximately twice as fast as that of the puller–pusher. This is because the flow field of a pusher–puller dumbbell tends to become more fore-and-aft asymmetric than that of other dumbbells, inducing a significant hydrodynamic self-propulsion force. Moreover, the pusher–puller dumbbell induces flows, which is more beneficial in the positive superposition for driving the body.

Additionally, we find swimming in a viscoelastic fluid expends less energy than its Newtonian counterpart, and the fluid inertia results in a decrease of energy expenditure. The energy expenditure is shown to be relevant at steady swimming speeds, in which the faster counterpart squirmer (dumbbell) expends less energy. The hydrodynamic efficiency

η increases monotonically with Re, and also with Wi. This pattern also displays a positive relationship with the swimming speed of the counterpart swimmers.

Funding. The authors would like to thank the Major Program of National Natural Science Foundation of China (Grant Nos. 12132015) and National Natural Science Foundation of China (Grant Nos. 12172327; 11972203).

Declaration of interests. The authors report no conflict of interest.

Data availability. The data that support the findings of this study are available from the corresponding author upon reasonable request.

Author ORCIDs.
Zhenyu Ouyang http://orcid.org/0000-0002-2481-0994;
Jianzhong Lin http://orcid.org/0000-0001-8418-1176.

Appendix A. On the details of solving (2.6)

The set of equations related to $\boldsymbol{\Lambda}$ have the following forms:

$$\left.\begin{aligned}\frac{\partial \tilde{l}_{ii}}{\partial t} &= g_{ii} - \boldsymbol{u}\cdot\nabla\tilde{l}_{ii},\\ \frac{\partial l_{ij(j>i)}}{\partial t} &= g_{ij} - \boldsymbol{u}\cdot\nabla l_{ij},\end{aligned}\right\} \tag{A1}$$

where the details of g_{ij} read as

$$\left.\begin{aligned}
g_{11} &= \frac{1}{2}\,\mathrm{e}^{(-2\tilde{l}_{11})}c_{11},\\
g_{21} &= \mathrm{e}^{(-\tilde{l}_{11})}c_{12} - \frac{l_{21}}{2}\,\mathrm{e}^{(-2\tilde{l}_{11})}c_{11},\\
g_{31} &= \mathrm{e}^{(-\tilde{l}_{11})}c_{13} - \frac{l_{31}}{2}\,\mathrm{e}^{(-2\tilde{l}_{11})}c_{11},\\
g_{22} &= \frac{1}{2}\,\mathrm{e}^{(-2\tilde{l}_{22})}c_{22} - l_{21}\,e^{(-\tilde{l}_{11}-2\tilde{l}_{22})}c_{12} + \frac{1}{2}l_{21}^2\,e^{(-2\tilde{l}_{11}-2\tilde{l}_{22})}c_{11},\\
g_{32} &= \mathrm{e}^{(-\tilde{l}_{22})}c_{23} - \frac{l_{32}}{2}\,\mathrm{e}^{(-2\tilde{l}_{22})}c_{22} - l_{21}\,\mathrm{e}^{(-\tilde{l}_{11}-\tilde{l}_{22})}c_{13} - (l_{22}l_{31} - l_{21}l_{32})\,\mathrm{e}^{(-\tilde{l}_{11}-2\tilde{l}_{22})}c_{12}\\
&\quad + \frac{1}{2}[2l_{21}\,\mathrm{e}^{(\tilde{l}_{22})}l_{31} - l_{21}^2 l_{32}]\,\mathrm{e}^{(-2\tilde{l}_{11}-2\tilde{l}_{22})}c_{11},\\
g_{33} &= \frac{1}{2}\,\mathrm{e}^{(-2\tilde{l}_{33})}c_{33} - l_{32}\,\mathrm{e}^{(-\tilde{l}_{22}-2\tilde{l}_{33})}c_{23} + \frac{l_{32}^2}{2}\,\mathrm{e}^{(-2\tilde{l}_{22}-2\tilde{l}_{33})}c_{22}\\
&\quad - [\mathrm{e}^{(\tilde{l}_{22})}l_{31} - l_{21}l_{32}]\,\mathrm{e}^{(-\tilde{l}_{11}-\tilde{l}_{22}-2\tilde{l}_{33})}c_{13}\\
&\quad + l_{32}[\mathrm{e}^{(\tilde{l}_{22})}l_{31} - l_{21}l_{32}]\,\mathrm{e}^{(-\tilde{l}_{11}-2\tilde{l}_{22}-2\tilde{l}_{33})}c_{12}\\
&\quad + \frac{1}{2}[\mathrm{e}^{(2\tilde{l}_{22})}l_{31}^2 - 2l_{21}\,\mathrm{e}^{(\tilde{l}_{22})}l_{31}l_{32} + l_{21}^2 l_{32}^2]\,\mathrm{e}^{(-2\tilde{l}_{11}-2\tilde{l}_{22}-2\tilde{l}_{33})}c_{11},
\end{aligned}\right\} \tag{A2}$$

with

$$\left.\begin{aligned}
c_{11} &= 2\left(b_{11}\frac{\partial u}{\partial x} + b_{12}\frac{\partial u}{\partial y} + b_{13}\frac{\partial u}{\partial z}\right) \\
&\quad - \frac{1}{Wi}[\alpha(b_{11}^2 + b_{12}^2 + b_{13}^2) + (1-2\alpha)b_{11} - (1-\alpha)], \\
c_{12} &= \left[\left(b_{11}\frac{\partial v}{\partial x} + b_{12}\frac{\partial v}{\partial y} + b_{13}\frac{\partial v}{\partial z}\right) + \left(b_{12}\frac{\partial u}{\partial x} + b_{22}\frac{\partial u}{\partial y} + b_{23}\frac{\partial u}{\partial z}\right)\right] \\
&\quad - \frac{1}{Wi}[\alpha(b_{11}b_{12} + b_{12}b_{22} + b_{13}b_{23}) + (1-2\alpha)b_{12}], \\
c_{13} &= \left[\left(b_{11}\frac{\partial w}{\partial x} + b_{12}\frac{\partial w}{\partial y} + b_{13}\frac{\partial w}{\partial z}\right) + \left(b_{13}\frac{\partial u}{\partial x} + b_{23}\frac{\partial u}{\partial y} + b_{33}\frac{\partial u}{\partial z}\right)\right] \\
&\quad - \frac{1}{Wi}[\alpha(b_{11}b_{13} + b_{12}b_{23} + b_{13}b_{33}) + (1-2\alpha)b_{13}], \\
c_{22} &= 2\left(b_{12}\frac{\partial v}{\partial x} + b_{22}\frac{\partial v}{\partial y} + b_{23}\frac{\partial v}{\partial z}\right) \\
&\quad - \frac{1}{Wi}[\alpha(b_{12}^2 + b_{22}^2 + b_{23}^2) + (1-2\alpha)b_{22} - (1-\alpha)], \\
c_{23} &= \left[\left(b_{12}\frac{\partial w}{\partial x} + b_{22}\frac{\partial w}{\partial y} + b_{23}\frac{\partial w}{\partial z}\right) + \left(b_{13}\frac{\partial v}{\partial x} + b_{23}\frac{\partial v}{\partial y} + b_{33}\frac{\partial v}{\partial z}\right)\right] \\
&\quad - \frac{1}{Wi}[\alpha(b_{12}b_{13} + b_{22}b_{23} + b_{23}b_{33}) + (1-2\alpha)b_{23}], \\
c_{33} &= 2\left(b_{13}\frac{\partial w}{\partial x} + b_{23}\frac{\partial w}{\partial y} + b_{33}\frac{\partial w}{\partial z}\right) \\
&\quad - \frac{1}{Wi}[\alpha(b_{13}^2 + b_{23}^2 + b_{33}^2) + (1-2\alpha)b_{33} - (1-\alpha)].
\end{aligned}\right\} \tag{A3}$$

References

Beckett, B.S. 1986 *Biology: A Modern Introduction*. Oxford University Press.

Binagia, J.P., Phoa, A., Housiadas, K.D. & Shaqfeh, E.S. 2020 Swimming with swirl in a viscoelastic fluid. *J. Fluid Mech.* **900**, A4.

Blake, J.R. 1971 A spherical envelope approach to ciliary propulsion. *J. Fluid Mech.* **46** (1), 199–208.

Cates, M.E. & MacKintosh, F.C. 2011 Active soft matter. *Soft Matter* **7** (7), 3050–3051.

Childress, S. 1981 *Mechanics of Swimming and Flying*. Cambridge University Press.

Chisholm, N.G., Legendre, D., Lauga, E. & Khair, A.S. 2016 A squirmer across Reynolds numbers. *J. Fluid Mech.* **796**, 233–256.

Clopés, J., Gompper, G. & Winkler, R.G. 2020 Hydrodynamic interactions in squirmer dumbbells: active stress-induced alignment and locomotion. *Soft Matter* **16** (47), 10676–10687.

Clopés, J., Gompper, G. & Winkler, R.G. 2022 Alignment and propulsion of squirmer pusher–puller dumbbells. *J. Chem. Phys.* **156** (19), 194901.

Costerton, J.W., Cheng, K.J., Geesey, G.G., Ladd, T.I., Nickel, J.C., Dasgupta, M. & Marrie, T.J. 1987 Bacterial biofilms in nature and disease. *Annu. Rev. Microbiol.* **41** (1), 435–464.

DASGUPTA, M., LIU, B., FU, H.C., BERHANU, M., BREUER, K.S., POWERS, T.R. & KUDROLLI, A. 2013 Speed of a swimming sheet in Newtonian and viscoelastic fluids. *Phys. Rev.* E **87** (1), 013015.

DATT, C., NATALE, G., HATZIKIRIAKOS, S.G. & ELFRING, G.J. 2017 An active particle in a complex fluid. *J. Fluid Mech.* **823**, 675–688.

ELFRING, G.J. & GOYAL, G. 2016 The effect of gait on swimming in viscoelastic fluids. *J. Non-Newtonian Fluid Mech.* **234**, 8–14.

GAO, W. & WANG, J. 2014 Synthetic micro/nanomotors in drug delivery. *Nanoscale* **6** (18), 10486–10494.

GÖTZE, I.O. & GOMPPER, G. 2010 Mesoscale simulations of hydrodynamic squirmer interactions. *Phys. Rev.* E **82** (4), 041921.

HARMAN, M.W., DUNHAM-EMS, S.M., CAIMANO, M.J., BELPERRON, A.A., BOCKENSTEDT, L.K., FU, H.C., RADOLF, J.D. & WOLGEMUTH, C.W. 2012 The heterogeneous motility of the Lyme disease spirochete in gelatin mimics dissemination through tissue. *Proc. Natl Acad. Sci.* **109** (8), 3059–3064.

HOUSIADAS, K.D. 2021 An active body in a phan-thien and tanner fluid: the effect of the third polar squirming mode. *Phys. Fluids* **33** (4), 043110.

HOUSIADAS, K.D., BINAGIA, J.P. & SHAQFEH, E.S.G. 2021 Squirmers with swirl at low Weissenberg number. *J. Fluid Mech.* **911**, A16.

ISHIKAWA, T. 2019 Stability of a dumbbell micro-swimmer. *Micromachines* **10** (1), 33.

ISHIKAWA, T., LOCSEI, J.T. & PEDLEY, T.J. 2008 Development of coherent structures in concentrated suspensions of swimming model micro-organisms. *J. Fluid Mech.* **615**, 401–431.

ISHIKAWA, T. & PEDLEY, T.J. 2008 Coherent structures in monolayers of swimming particles. *Phys. Rev. Lett.* **100** (8), 088103.

ISHIKAWA, T., SIMMONDS, M.P. & PEDLEY, T.J. 2006 Hydrodynamic interaction of two swimming model micro-organisms. *J. Fluid Mech.* **568**, 119–160.

ISHIMOTO, K. & GAFFNEY, E.A. 2013 Squirmer dynamics near a boundary. *Phys. Rev.* E **88** (6), 062702.

KATZ, D.F. & BERGER, S.A. 1980 Flagellar propulsion of human sperm in cervical mucus1. *Biorheology* **17** (1–2), 169–175.

KHAIR, A.S. & CHISHOLM, N.G. 2014 Expansions at small Reynolds numbers for the locomotion of a spherical squirmer. *Phys. Fluids* **26** (1), 011902.

KIØRBOE, T., JIANG, H. & COLIN, S.P. 2010 Danger of zooplankton feeding: the fluid signal generated by ambush-feeding copepods. *Proc. R. Soc.* B*: Biol. Sci.* **277** (1698), 3229–3237.

LESHANSKY, A.M. 2009 Enhanced low-Reynolds-number propulsion in heterogeneous viscous environments. *Phys. Rev.* E **80** (5), 051911.

LI, C., QIN, B., GOPINATH, A., ARRATIA, P.E., THOMASES, B. & GUY, R.D. 2017*a* Flagellar swimming in viscoelastic fluids: role of fluid elastic stress revealed by simulations based on experimental data. *J. R. Soc. Interface* **14** (135), 20170289.

LI, G., LAUGA, E. & ARDEKANI, A.M. 2021 Microswimming in viscoelastic fluids. *J. Non-Newtonian Fluid Mech.* **297**, 104655.

LI, G., OSTACE, A. & ARDEKANI, A.M. 2016 Hydrodynamic interaction of swimming organisms in an inertial regime. *Phys. Rev.* E **94** (5), 053104.

LI, G.-J., KARIMI, A. & ARDEKANI, A.M. 2014 Effect of solid boundaries on swimming dynamics of microorganisms in a viscoelastic fluid. *Rheol. Acta* **53** (12), 911–926.

LI, J., ESTEBAN-FERNÁNDEZ DE ÁVILA, B., GAO, W., ZHANG, L. & & WANG, J. 2017*b* Micro/nanorobots for biomedicine: delivery, surgery, sensing, and detoxification. *Sci. Robot.* **2** (4), eaam6431.

LIGHTHILL, M.J. 1952 On the squirming motion of nearly spherical deformable bodies through liquids at very small Reynolds numbers. *Commun. Pure Appl. Math.* **5** (2), 109–118.

LIN, Z. & GAO, T. 2019 Direct-forcing fictitious domain method for simulating non-Brownian active particles. *Phys. Rev.* E **100** (1), 013304.

MAGAR, V., GOTO, T. & PEDLEY, T.J. 2003 Nutrient uptake by a self-propelled steady squirmer. *Q. J. Mech. Appl. Maths* **56** (1), 65–91.

MAGAR, V. & PEDLEY, T.J. 2005 Average nutrient uptake by a self-propelled unsteady squirmer. *J. Fluid Mech.* **539** (1), 93–112.

MORE, R.V. & ARDEKANI, A.M. 2020 Motion of an inertial squirmer in a density stratified fluid. *J. Fluid Mech.* **905**, A9.

NAVARRO, R.M. & PAGONABARRAGA, I. 2010 Hydrodynamic interaction between two trapped swimming model micro-organisms. *Eur. Phys. J.* E **33** (1), 27–39.

NGANGUIA, H., ZHENG, K., CHEN, Y., PAK, O.S. & ZHU, L. 2020 A note on a swirling squirmer in a shear-thinning fluid. *Phys. Fluids* **32** (11), 111906.

OUYANG, Z. & LIN, J. 2021 The hydrodynamics of an inertial squirmer rod. *Phys. Fluids* **33** (7), 073302.

OUYANG, Z., LIN, J. & KU, X. 2018*a* Hydrodynamic properties of squirmer swimming in power-law fluid near a wall. *Rheol. Acta* **57** (10), 655–671.

OUYANG, Z., LIN, J. & KU, X. 2018*b* The hydrodynamic behavior of a squirmer swimming in power-law fluid. *Phys. Fluids* **30** (8), 083301.

OUYANG, Z., LIN, J. & KU, X. 2019 Hydrodynamic interaction between a pair of swimmers in power-law fluid. *Intl J. Non-Linear Mech.* **108**, 72–80.

OUYANG, Z., LIN, Z., LIN, J., YU, Z. & PHAN-THIEN, N. 2023 Cargo carrying with an inertial squirmer in a Newtonian fluid. *J. Fluid Mech.* **959**, A25.

OUYANG, Z., LIN, Z., YU, Z., LIN, J. & PHAN-THIEN, N. 2022 Hydrodynamics of an inertial squirmer and squirmer dumbbell in a tube. *J. Fluid Mech.* **939**, A32.

OUYANG, Z. & PHAN-THIEN, N. 2021 Inertial swimming in a channel filled with a power-law fluid. *Phys. Fluids* **33** (11), 113312.

PAK, O.S., ZHU, L.L., BRANDT, L. & LAUGA, E. 2012 Micropropulsion and microrheology in complex fluids via symmetry breaking. *Phys. Fluids* **24** (10), 103102.

PATTESON, A.E., GOPINATH, A., GOULIAN, M. & ARRATIA, P.E. 2015 Running and tumbling with *E. coli* in polymeric solutions. *Sci. Rep.* **5** (1), 15761.

PEDLEY, T.J., BRUMLEY, D.R. & GOLDSTEIN, R.E. 2016 Squirmers with swirl: a model for volvox swimming. *J. Fluid Mech.* **798**, 165–186.

SANCHEZ, T., CHEN, D.T., DECAMP, S.J., HEYMANN, M. & DOGIC, Z. 2012 Spontaneous motion in hierarchically assembled active matter. *Nature* **491** (7424), 431–434.

SCHALLER, V., WEBER, C., SEMMRICH, C., FREY, E. & BAUSCH, A.R. 2010 Polar patterns of driven filaments. *Nature* **467** (7311), 73–77.

SMITH, D.J., GAFFNEY, E.A., GADÊLHA, H., KAPUR, N. & KIRKMAN-BROWN, J.C. 2009 Bend propagation in the flagella of migrating human sperm, and its modulation by viscosity. *Cell Motil Cytoskel.* **66** (4), 220–236.

VAITHIANATHAN, T. & COLLINS, L.R. 2003 Numerical approach to simulating turbulent flow of a viscoelastic polymer solution. *J. Comput. Phys.* **187** (1), 1–21.

WANG, S. & ARDEKANI, A. 2012 Inertial squirmer. *Phys. Fluids* **24** (10), 101902.

WENSINK, H.H., DUNKEL, J., HEIDENREICH, S., DRESCHER, K., GOLDSTEIN, R.E., LÖWEN, H. & YEOMANS, J.M. 2012 Meso-scale turbulence in living fluids. *Proc. Natl Acad. Sci.* **109** (36), 14308–14313.

WICKRAMARATHNA, L.N., NOSS, C. & LORKE, A. 2014 Hydrodynamic trails produced by daphnia: size and energetics. *PLoS ONE* **9** (3), e92383.

WINKLER, R.G. & GOMPPER, G. 2020 The physics of active polymers and filaments. *J. Chem. Phys.* **153** (4), 040901.

YAN, X., ZHOU, Q., VINCENT, M., DENG, Y., YU, J., XU, J., XU, T., TANG, T., BIAN, L., WANG, Y.-X.J., KOSTARELOS, K. & ZHANG, L. 2017 Multifunctional biohybrid magnetite microrobots for imaging-guided therapy. *Sci. Robot.* **2** (12), eaaq1155.

YU, Z. & SHAO, X. 2007 A direct-forcing fictitious domain method for particulate flows. *J. Comput. Phys.* **227** (1), 292–314.

YU, Z., WANG, P., LIN, J. & HU, H.H. 2019 Equilibrium positions of the elasto-inertial particle migration in rectangular channel flow of Oldroyd-B viscoelastic fluids. *J. Fluid Mech.* **868**, 316–340.

ZANTOP, A.W. & STARK, H. 2020 Squirmer rods as elongated microswimmers: flow fields and confinement. *Soft Matter* **16** (27), 6400–6412.

ZHU, L., DO-QUANG, M., LAUGA, E. & BRANDT, L. 2011 Locomotion by tangential deformation in a polymeric fluid. *Phys. Rev.* E **83** (1), 011901.

ZHU, L., LAUGA, E. & BRANDT, L. 2012 Self-propulsion in viscoelastic fluids: pushers vs. pullers. *Phys. Fluids* **24** (5), 051902.

ZÖTTL, A. & STARK, H. 2014 Hydrodynamics determines collective motion and phase behavior of active colloids in quasi-two-Dimensional confinement. *Phys. Rev. Lett.* **112** (11), 118101.